Electromagnetic Excitation for Blade Vibration Analysis in Static Conditions: Theoretical Insights and Experimental Evaluation

Mohammed Lamine Mekhalfia*[(a)], Pavel Procházka [(a)] , Radislav Smid [(b)], Philip Bonello [(c)], Peter Russhard [(d)], Dušan Maturkanič [(a)] , Mohamed Elsayed Mohamed [(e)] and Eder Batista Tchawou Tchuisseu [(a)].

[(a)] Dept. Dynamics and Vibration
Institute of Thermomechanics of the CAS
Prague, Czech Republic

[(b)] FEE
Czech Technical University in Prague
Prague, Czech Republic

[(c)] Dept. Mechanical and Aerospace Engineering
University of Manchester
United Kingdom

[(d)] EMTD LTD
United Kingdom

[(e)] School of Engineering and Computing
University of Central Lancashire
United Kingdom

***Abstract*—Blade vibration testing is crucial for understanding the dynamic behavior of rotating machinery. This paper presents a theoretical analysis and experimental validation of electromagnetic excitation for blade vibration testing in static conditions. The study focuses on investigating the effect of electromagnets on static blades to establish a theoretical foundation. The Timoshenko beam theory is utilized to analyze the vibration parameters, including amplitude and frequency, while considering associated uncertainties. The theoretical analysis is complemented by numerical modeling using the finite element method and experimental measurements employing Laser Doppler Vibrometry (LDV). The results demonstrate the effectiveness of electromagnetic excitation in generating controlled vibrations in static blades. These findings provide valuable insights and serve as a basis for subsequent investigations into the behavior of blades during rotation. The mathematical model's frequency estimation error was approximately 4% compared to numerical results, and the numerical amplitude results differed by 6.4% from the experimental measurements. These contributions enhance the understanding and design of blade vibration monitoring systems in rotating machinery and provide valuable information on the blade's dynamic parameters for the calibration of blade tip timing systems.**

***Index Terms*—Aero-compressor blade, Magnetic excitation, static blade, vibration parameters.**

I. Introduction

In turbomachines, blade vibrations predominantly arise due to demanding operational factors such as aerodynamic forces, pressure and speed fluctuations, resonances, mechanical imbalances and coupling, blade deterioration, operational conditions and regimes, etc [1], [2]. Excessive vibrations reduce the operating service life of the blades by affecting their structural dynamics and stiffness [3]. If blade vibration is not properly controlled, monitored, and limited, blade break-off can occur resulting in severe damage to the turbomachine with huge economic losses [4]–[7].

Over the years, numerous methods have been developed for measuring blade vibrations under rotation, broadly categorized into two groups: contact methods using strain gauges and non-contact methods based on optical measurements (Laser Doppler Velocimetry "LDV") or precise time measurements of blade passages under stator sensors, the so-called Blade Tip Timing (BTT) method [8]. Blade tip timing systems are becoming increasingly involved in operational blade vibration monitoring. The BTT concept relies on determining the arrival time of the blades using non-contact probes.

In Blade Tip Timing (BTT) systems, there are technical limitations that restrict the number of probes that can be used. Consequently, the signals we obtain are undersampled. Reconstructing vibration from the measured signals may involve ambiguity, necessitating prior assumptions or knowledge about the frequencies and amplitudes determined by blade dynamics. This knowledge is also essential when aiming to minimize measurement errors and determine the optimal probe positions [9]–[11].

The blade vibration can be either synchronous or asynchronous, which is determined by the frequency of the force exerted on the blade. Some of the current experimental equipment for testing and optimizing BTT systems provides an enhanced excitation system and operates with both types of vibrations [12]–[14]. The excitation systems used in current technical practice are mostly based on the force effects of an air jet or an electromagnetic field. In this article, we will deal with the electromagnetic excitation systems. Since the blade is ferromagnetic, the magnetic pulling force is decisive for the excitation of its vibrations.

Despite extensive research in the field of blade vibration analysis, most existing studies predominantly focus on either non-destructive testing methods or the dynamics of rotating blades [15]–[17]. While non-destructive testing methods provide valuable insights into material integrity and structural health, they do not specifically address the dynamic behavior of blades under controlled excitation [18]–[23]. Similarly, research on rotating blade dynamics often emphasizes operational conditions without isolating the influence of electromagnetic excitation in static scenarios. Thus Our study uniquely contributes to the field by providing a comprehensive theoretical and experimental analysis of blade vibrations induced by electromagnetic excitation in static conditions. This foundational work is essential for subsequent investigations into the behavior of blades during rotation, offering a new

* Corresponding author. Email: m.mekhalfia@it.cas.cz

perspective on blade dynamics that has not been extensively covered in prior research.

The article presents a theoretical analysis of the vibration of steam turbine blades verified numerically and experimentally. In this work, we model the blade geometry considering it to be twisted and untwisted, and then study its dynamics under magnetic excitation by an electromagnet. Our proposed solution contains a basic algorithm for solving the mathematical model and determining the blade dynamics. At the end of the research process, the results are compared with those obtained using ANSYS, as well as with the results of experimental measurements obtained using LDV.

The article structure is as follows: In Section II, we describe the system and present the equivalent mathematical model, resulting in determining the natural frequencies of the blade modeled as a cantilever beam. The numerical analysis performed using the fourth-order Runge-Kutta in combination with the finite difference method to study the dynamics of the excited blade. Section III deals with the validation process of the mathematical analysis using FEM applied through ANSYS and by the LDV experimental measurements; the results are analyzed and discussed here. The final section provides an overall summary and conclusions of the study.

II. Electromagnetic Force Modeling for Cantilevered Blade Vibration

The system under investigation is an electro-mechanical system shown in Fig. 1 (a). The mechanical component is a flexible ferromagnetic blade made of steel. An electromagnet is considered the electrical portion of the system. The electromagnet consists of a coil and a wound wire connected to a power unit to control the supplied electric current. If the electromagnet is not saturated, the electric current supplied by the power source flows across the coil, generating a magnetic field B, which is constant if the electric current is constant and time-varying if the electric current is time-varying. Thus, the created magnetic field induces a magnetic force F_m, which acts on the ferromagnetic blades. The form of the power source signal supplying the electromagnet develops a magnetic force of the same shape. When an electromagnet is powered with alternating current, the resulting alternating magnetic field induces periodic attraction and release of a nearby magnetic blade due to changes in magnetic polarity (Fig. 1 (b)), resulting in blade vibration.

A. Model for the electromagnetic force $F_E(w,t)$

The electromagnet shown in Fig. 1, is placed in front of the blade and develops a magnetic force when it is powered. The magnetic force generated by an electromagnet of N turns, magnetic induction B, cross-section A and powered by a current I_e is given by Eq. (1):

$$F_E(w,t) = \frac{B^2(w,t)A}{2\mu_0}. \tag{1}$$

Applying Hopkinson's law which gives the relationship between the reluctance of the magnetic circuit, the flux and the number of turns N through the magneto-motive force, we have:

$$F_E = NI_e = \mathcal{R}\Phi, \tag{2}$$

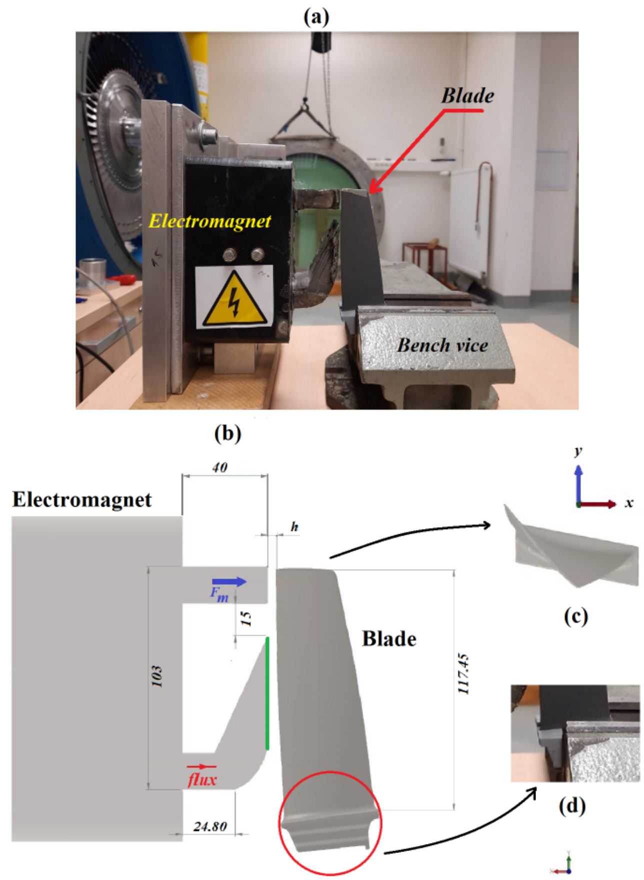

Fig. 1. (a): Blade-Electromagnet system, (b): Simplified schematic presentation of the system (c): Top view of the blade-electromagnet system with directions of movement indicated (d): detailed view n fixing the blade from the root using the bench vice (cantilever blade).

where I_e is the electric current, $\mathcal{R}$ denotes the total reluctance of the medium through which the magnetic flux Φ passes. Thus, the magnetic force applied to the blade is given by the equation:

$$F_E(w,t) = \frac{(NI_e(t))^2}{2\mu_0 A}\frac{1}{\mathcal{R}^2(w(x))}, \tag{3}$$

With the total reluctance given with:

$$\mathcal{R}(w(x)) = \frac{l_m}{\mu_m A} + \frac{h^{'} - w}{\mu_0 A} + \frac{l_b}{\mu_b A}, \tag{4}$$

l_m, l_b and $h^{'} - w$ represent the effective length traveled by the magnetic flux in the electromagnet, blade and air, respectively, w is the lateral vibration of the blade.
$\mu_m = \mu_{rm}\mu_0$ and $\mu_b = \mu_{bm}\mu_0$ are the magnetic permeability of the material component of the electromagnet and the blade, respectively, where μ_0 represents the magnetic permeability in vacuum.

$$F_E(w,t) = \frac{\mu_0 N^2 A}{2\left[(\frac{l_b}{\mu_{rb}}) + (\frac{l_m}{\mu_{rm}}) + h^{'} - w\right]^2} \times I_e^2. \tag{5}$$

In addition, we assume that the magnetic permeability of the blade and the ferromagnetic material are too large compared to the magnetic permeability of the air gap ($\mu_{rb} >> \mu_0$ and $\mu_{rb} >> \mu_0$). This implies $(\frac{l_b}{\mu_{rb}}) << (h^{'} - w)$ and $(\frac{l_m}{\mu_{rm}}) << (h^{'} - w)$. Thus, Eq. (5) can be rewritten as in [19]:

$$F_E(w(t), x) = \frac{\mu_0 N^2 A}{2\epsilon^2 \left(h^{'} - w\right)^2} \times I_e(t)^2, \tag{6}$$

where ϵ is a correction coefficient due to the assumption of the authors in [25]. In the following passages and for the sake of simplicity, we consider $\epsilon = 1$. N is the number of turns of the coil, $h^{'} = 2h + g(x)$ is the total length crossed by the magnetic flux, and h is the constant upper air-gap between the blade and the electromagnet the equilibrium. I is the current enabling the magnetization of the material. $g(x)$ is the gap between the bottom of the blade and the electromagnet. In fact, Fig. 1 shows that the two poles of the electromagnet have different shapes. The lower surface is pointed (green line in Fig. 1), so the gap between the blade and the electromagnet is determined by the following equation:

$$e(y) = my + b, \tag{7}$$

where x and u are the coordinates of random point on the blade in the system of axes considered here (y, x) as in Fig. 1 (c), m is the slope of the line, and b a constant. Considering our systems's coordinates, the upper point of the line is given by $A(y_A, x_A)$, the lowest point is given by $B(y_B, x_B)$. For this particular analysis, $y_A = h\ cm$, $x_A = 7.5\ cm$, $y_B = h + 1.4\ \ cm$, $x_B = 0\ cm$, and the constant gap $h = 0.2\ cm$. Thus, we obtain the following parameters of $m = -5.35$ and $b = 8.57$ of the red line (presented on the picture of the blade attached to Fig. 2 plot) . Accordingly, Eq. (7) can be written in its discrete form as follows:

$$e(y_i) = -5.35 y_i + 8.57 = x_i(cm) \tag{8}$$

The coordinates x_i are defined such that the blade is divided into n pieces represented by their position: $x_i = (i-1)/n$, with $i = 1, \ldots, n$. The Eq. (7) implies that the air-gap between the electromagnet and the blade is not constant. In fact, for $0 \leq x_i \leq x_A$ the gap varies according to the equation:

$$g(x_i) = \frac{x_i - b}{m}, \tag{9}$$

This gap is constant for $x > 7.5 \times 10^{-2}(m)$. This discontinuity in the air gap due to the blade vibration implies that the distribution of the magnetic force along the blade is not uniform. In addition, the electrical current I_e can be constant or time-varying. For a constant value of the electrical current, the magnetic field generated is constant; if the electrical current is high enough and in the absence of any force applied to the blade, the blade is attracted by the electromagnet and will remain at that position until the electric current is switched off. In the case time-varying current, there is a variation of the magnetic flux due to the variation of the magnetic field. This can be represented by the case where the current takes the form of a sine function: $I_e(t) = I_{max} cos(2\pi f_m t)$, with I_{max} and f_m, the maximum amplitude and the frequency of the current respectively. When the blade is close enough to the electromagnet, the variation of flux induces eddy currents, creating a new magnetic field opposite to the one generated by the electromagnet. This induced magnetic field modifies the current and it modifies also the inductive reactance of the electromagnet coil. The Inductive reactance is represented by X_L=$2\pi f_m L$ (Ω), with L (H) being the inductance of the coil of the electromagnets. As a side effect, the eddy currents circulating across the blade (conductor with a resistance R) produce heat loss on the conductor, whose temperature increases. This effect (Eddy currents) is controlled by a stabilizer, which ensures that the coil's inductive reactance remains constant. In the absence of such a controller, the dynamics of the induced current i_b in the coil of the electromagnet would be given by the following equation:

$$L_b \frac{\partial i_b}{\partial t} + R i_b = B l_b \frac{\partial w}{\partial t} \tag{10}$$

where L_b, l_b and R are the inductance, length, and resistance of the coil of the electromagnet, B is the magnetic field created by the current $i_b(t)$ and $w(t)$ is the transverse displacement of the blade. This current i_b in the case of a permanent supply of the electromagnet by a current I_{max} can be measured following the principle detailed in [15] if the blade in motion due to an external force. This case can be seen when the blade is rotating, since the rotation of the blade generates a centrifugal force proportional to the square of the blade rotation speed.

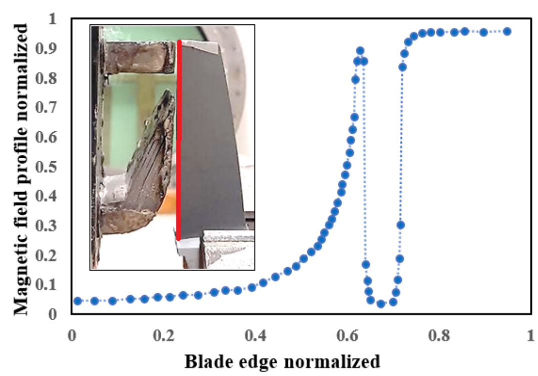

Fig. 2. Simplified normalized magnetic field profile along the blade edge facing the electromagnet - The blade edge was highlighted in red.

The electric current supplying the electromagnet is assumed to be alternating current; thus, the corresponding attractive force developed given by Eq. (11) is alternating, and oscillating at twice the frequency compared to the current frequency.

$$F(w, t) = F_{E_{max}} \cos^2(2\pi f_m t) \tag{11}$$

where f_m is the frequency of the AC current $(I_e(t) = I_{max}\cos(2\pi f_m t))$, $F_E(w)$ is the amplitude of the magnetic force defined by:

$$F_{E_{\max}}(w(t), x) = \frac{\mu_0 N^2 A I_{\max}^2}{2(2h + g(x) - w(t))^2} \tag{12}$$

where I_{max} is the amplitude of the current supplying the electromagnet. The magnetic force applied to the blade is found to be non-uniform. The experimental determination of the magnetic field created by the electromagnet can be achieved by inserting a magnetometer at several points near the blade edge. The measured magnetic field along the blade tip has a non-uniform distribution or profile as shown in Fig. 2. The experimental results of the magnetic field are consistent with the amplitude of the magnetic force given in Eq.(12).

B. Blade geometry and parameters

In the below expression of the frequency obtained from the Timoshenko model [24]:

$$f_k = \frac{\lambda_k^2}{2\pi L^2}\sqrt{\frac{EI}{\rho S}} \tag{13}$$

where f_k is the angular natural frequency of the blade in Hz, the parameter k denotes the mode of vibration and the mode parameter λ_k, E is the young Modulus, L is the Blade length and ρ is the material density. the blade cross-section S and the second moment of area I are assumed constant, which is an adequate assumption for a uniform blade. Turbine blades, in general, are twisted with airfoil profiles. The blade used in this study was extracted from the bladed disc assembly of the Viper 522 used by the authors of this article in the BATISTA project. The blade is characterized by its specific dimensions and material properties, which are detailed in the paper on section II-C (under Eq. (16)). The chosen geometry is representative of typical steam turbine blades and shown in Fig. 3 (a). Numerical simulation was used to ensure the propreties of the particular blade. For simplicity in this theoretical analysis, a visual comparison of the blade profile with the existing ones obtained from [25] shows that the current profile has originated probably from the R.A.F 6 (see Fig. 3 (b)) and modified. This means that the maximum thickness 10 % at 30 % chord and the maximum camber is 4.6 % at 30% chord [25].

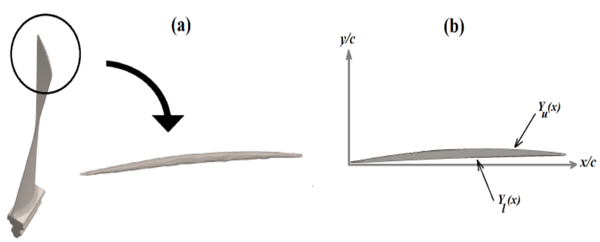

Fig. 3. (a) BATISTA blade with top view -(b) R.A.F 6 airfoil profile from data obtained in [25].

Thus, defining $Y_u(x)$ and $Y_l(x)$ as the upper and lower curves of the blade cross-section respectively, we can mathematically define the following geometrical characteristics of the blade: The area $S(x)$, the maximal thickness ξ and the maximal camber c_{max} of the blade cross-section given by Eq. (14) and Eq. (15), respectively.

$$\begin{aligned} S &= \int_0^C (Y_u(x) - Y_l(x))dx \\ \xi &= max(Y_u(x) - Y_l(x)) \times c \\ c_{max} &= max((Y_u(x) + Y_l(x))/2) \times c \end{aligned} \tag{14}$$

Thus, the area and the second moment of area of the airfoil cross-section about the bending axis can be given by the following expressions:

$$\begin{aligned} S &\simeq K_S c\xi \\ I &\simeq K_I c\xi(\xi^2 + c_{max}^2), \end{aligned} \tag{15}$$

K_S and K_I are parameters depending on the area and the moment of inertia of the airfoil cross-section respectively. Their values are almost the same for the common airfoils as reported by [26]: $K_S = 0.6$ and $K_I = 0.036$. The blade considered in this work has as chord $c = 0,0414\ m$. Thus, we obtain the following approximations of the blade geometrical properties: I=$10.78 \times 10^{-12}\ m^4$ and S=$47.30 \times 10^{-6}\ m^2$.

C. Numerical Analysis of Electromagnetic-Induced Vibration

We used the Fourier transform of the blade tip displacement to dynamically analyze our system by plotting the displacement history. This allows the blade tip vibration frequency to be identified. We used the phase portrait combined with the Poincare map, where the phase portrait gives the trajectory of the blade in the phase plane and the Poincare map marks in the phase plane the position of the blade at each defined time period. The governing motion equations of the excited blade derived from the Timoshenko model are numerically solved using the fourth-order Runge-Kutta method coupled to the centered difference methods as given by the expression below. The time step $d\tau = 1 \times 10^{-7}$ and the spatial step Δx=$1/n$, where n is the number of points chosen along the blade. $t_j = j \times d\tau$ represents the discretized time.

$$\begin{aligned} &\frac{(w_{i,j+1}-2w_{i,j}+w_{i,j-1})}{d\tau^2} \\ &+\Big(\frac{EI(w_{i+2,j}+2w_{i-2,j}-4(w_{i+1,j}+w_{i-1,j})+6w_{i,j})}{\rho S\Delta x^4}\Big]\Big) \\ &-\rho I\left(1+\frac{E}{\kappa G}\right) \\ &\Big[\frac{(w_{i+1,j+1}-2w_{i+1,j}+w_{i+1,j-1})}{S\Delta x^4 d\tau^2} \\ &-\frac{2(w_{i,j+1}-2w_{i,j}+w_{i,j-1})}{S\Delta x^4 d\tau^2} \\ &+\frac{(w_{i-1,j+1}-2w_{i-1,j}+w_{i-1,j-1})}{S\Delta x^4 d\tau^2}\Big] \\ &+\frac{\rho I}{\kappa GS}\frac{(w_{i,j+2}+2w_{i,j-2}-4(w_{i,j+1}+w_{i,j-1})+6w_{i,j})}{d\tau^2} \\ &=\frac{1}{\rho S}\Bigg[F_i\cos^2(2\pi f_m t_j)+\frac{EI}{\kappa SG}\Bigg[\left(\frac{\partial^2 F(x,t)}{\partial t^2}\right)_{i,j} \\ &\quad-\left(\frac{\partial^2 F(x,t)}{\partial x^2}\right)_{i,j}\Bigg]\Bigg]. \end{aligned} \tag{16}$$

The numerical simulation of Eq.(16) was carried out considering the following parameters: L (length of the blade)= $0.118\ m$; ρ (volume density)= 7700 $Kg.m^{-3}$; S (blade cross-section)= $47.3 \times 10^{-6}\ m^2$; I (second moment of area about the x axis)= $10,78 \times 10^{-12}\ m^4$; E (Young modulus)= 210 GPa, n= 50 elements, and the initial gap $h = 2 \times 10^{-3}\ m$. The blade's natural frequencies shown in Fig. 4 were obtained numerically by resolving Eq. (16) without excitation. The initial conditions were determined assuming a light bending of the blade so that the initial displacement of an element i can be expressed as follows:

$$w_{i,0} = -\frac{Px_i}{\kappa SG} + \frac{P{x_i}^3}{18EI}$$

with P=10^{-5} Pa representing the pressure exerted on the blade due to its inertia.

Fig. 4 (a) represents the blade displacement with respect to

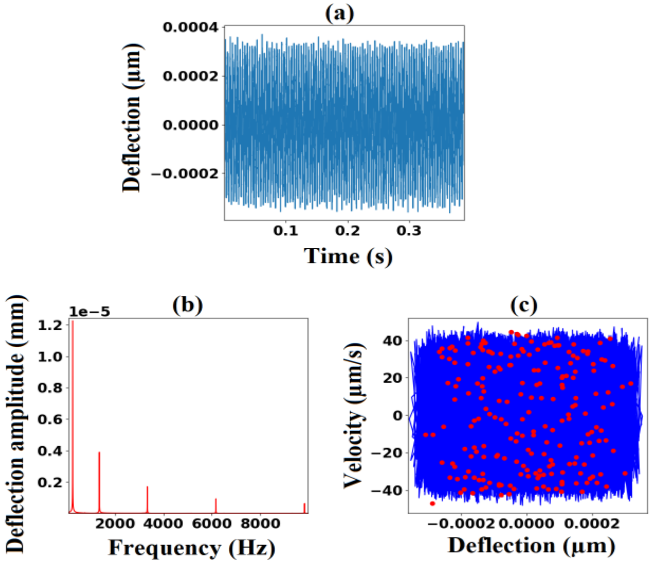

Fig. 4. (a) Time evolution of the blade's lateral deflection under initial conditions -No excitation, (b): Lateral deflection frequency spectrum, and (c): Phase portrait (in blue) and Poincare map (in red).

the initial conditions and the blade characteristics. We noted that the blade vibrates with many peaks, which implies that we can not define the dynamics of the blade by a single period. This result is confirmed by the power spectrum (b), the phase portrait (blue), and the Poincare map (red). The number of red dots defines the number of frequencies present in the dynamics of the blade. The most significant first four frequencies are: $\omega_1^0 = 351\ Hz, \omega_2^0 = 1154\ Hz, \omega_3^0 = 3335\ Hz$ and $\omega_4^0 = 6168$ Hz. In the subsequent results, the system is assumed to be excited by a magnetic force generated when the alternating electric current with a frequency ω is flowing through the coils. The rest of the parameters remain unchanged. Thus, in Fig. 5 and 6, different behavior of the blade is observed by only modifying the frequency of excitation and preserving the same amplitude. Fig. 5 shows the blade deflection as a function of time (a) for the electromagnet powered by a current frequency $\omega = 46\ Hz$.

Fig. 5 presents many peaks, with the maximal amplitude of about 115 μm. The observed peaks reflect that the blade is not vibrating only with a single frequency. This observation is confirmed by the representation of the frequencies of vibration of the blade given in Fig. 5 (b). Two frequencies can be observed with the highest amplitude, meaning those frequencies are the most contributing to the dynamics of the blade, which are $\omega = 92\ Hz$ and $\omega = 351\ Hz$. It is worth mentioning that $\omega = 351\ Hz$ corresponds to the frequency of the first mode of vibration of the blade, and $\omega = 92\ Hz$ is induced by the excitation force of the same frequency. A blade when excited vibrates with infinite frequencies due to the harmonic nature of the alternating force used for the excitation. Fig. 5 (c) represents the phase portrait (blue) and the Poincare (red). The phase portrait reflects the behaviors of the blade, which can be taken at the first observation as chaotic behavior. The

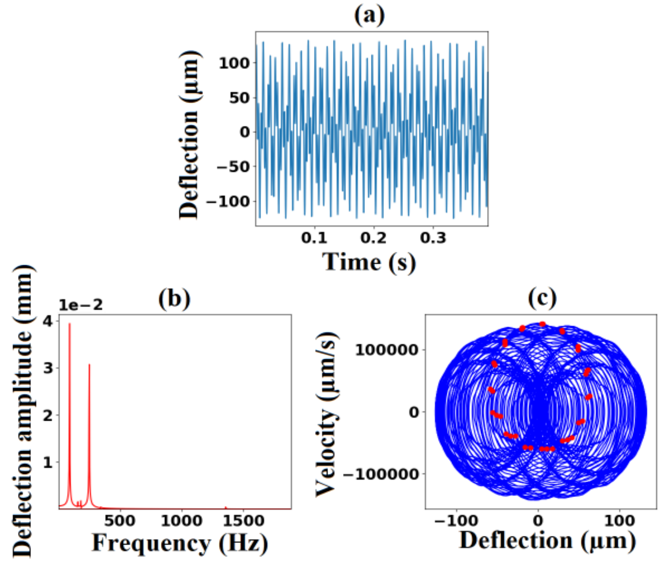

Fig. 5. (a): Time evolution of blade's lateral deflection due to the magnetic force generated by the electromagnet supplied by a current with frequency $\omega = 46\ Hz$, (b): Lateral deflection frequency spectrum, and (c): Phase portrait (in blue) and Poincare map (in red). The rest of the parameters of the system as indicated above.

Poincare map clarifies the type of the blade dynamics included in this case, the behavior is quasi-periodic, highlighted by the red ring. The quasi-periodicity could have been predicted by looking at the amplitude as a function of the frequency, which shows that the predominant vibration frequency of the blade vibrates quasi with the same amplitude.

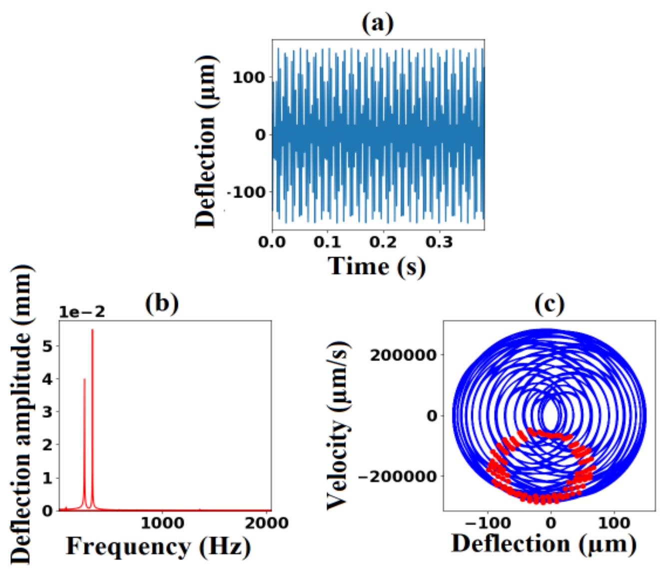

Fig. 6. (a): Time evolution of blade's lateral deflection due to the magnetic force generated by the electromagnet supplied by a current with frequency $\omega = 164\ Hz$, (b): Lateral deflection frequency spectrum and (c): Phase portrait (in blue) and Poincare map (in red). The rest of the parameters of the system as indicated above.

The same behavior of the blade was observed in Fig. 6 shows the case, where the frequency of excitation of the blade is now set to $\omega = 164\ Hz$. The time evolution of the lateral deflection in this case shows a quasi-periodic behavior of the blade dominated by the excitation frequency. This observation is confirmed by the phase portrait (in blue) and the Poincare map (in red), which forms a ring characteristic of quasi-periodic oscillations.

III. Validation and Comparison of Models

In the previous theoretical analysis, we presented the motion equation of the blade and the dynamics analysis, where for the assumed approximations it was possible to numerically extract the natural frequencies of the blade by applying the Timoshenko cantilever beam theory. However, this mathematical approach requires making assumptions about the blade geometry. In this section, we propose to perform numerical analysis using ANSYS followed by experimental measurement to record the dynamics of the cantilever blade and validate our mathematical approach. It is worth noting that this section considers the actual geometry of the blade without assuming the simplification of the mathematical model in the previous section. We used SOLIDWORKS to design and model the blade geometry into a 3D virtual format and then ANSYS to perform the structural analysis.

A. Finite Element Modeling and Analysis of Cantilevered Blade Vibration

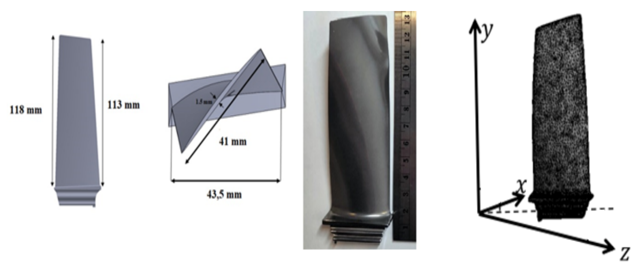

Fig. 7. The model of the blade.

The mesh used by ANSYS for this study conforms to tetrahedron patches.The size of the element used was 2.25 mm and the number of nodes was 24341. The modal analysis, which is the analysis to extract the natural frequencies and mode shapes of the blade, was performed using ANSYS, assuming that the blade was cantilevered, i.e. fixed at the root as in Fig. 1). The obtained results are shown in Fig. 8.

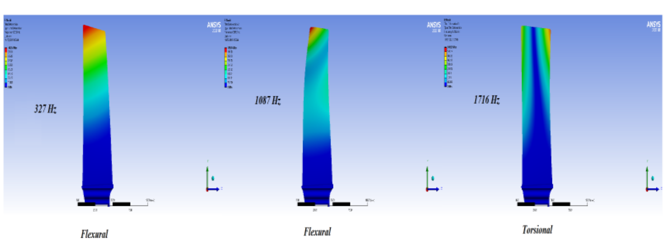

Fig. 8. Modal Analysis results for the 3 first mode via $ANSYS$.

A further step was performed using $ANSYS$ to simulate the magnetic force effect on the cantilevered blade; the force impact on the blade has the following characteristics is F_{max} = 93 N and 328 Hz, the amplitude chosen was calculated according to the following electromagnet characteristics: the section $S = 1.0371 \times 10^{-3} m^2$, the number of turns N = 160 and the inductance L=0.0031 H; see Fig. 9. The results that present the vibration of the tip obtained through a transient structural simulation by $ANSYS$ for the mentioned excitation are presented in Fig. 10.

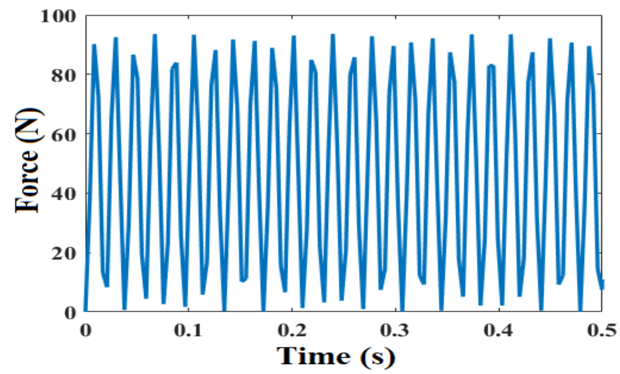

Fig. 9. Corresponding magnet excitation force.

B. Experimental Evaluation and Error Quantification

The experiment was performed according to the description in Fig. 1 (a). The blade was cantilevered with a fixed support parallel to the electromagnet that offers an alternating force F_{max} approximately equal to 93 N. This value was calculated from the electromagnet characteristics mentioned earlier and measured experimentally using an equivalent electromagnet using a load cell situated in the opposite side of the blade and assuming that the force is equal on both sides of the magnet. This force is presented in Fig. 9 and resulted from a supplied electrical current I_{max} = 25.5 A. The measurement was carried out by the Laser Doppler Vibrometer, which is a tool that measures vibration [27], [28]. We used a Laser Scanning Vibrometer Polytec PSV-500 [29]. It is worth mentioning that the vibrometer used is equipped with a derotator and a reference Vibrometer Polytec OFV-5000 This makes it suitable for future studies on magnetic excitation for blades under rotation. We positioned the scanning point at the blade's tip to ensure a comparable case between the numerical and experimental results.

The displacement curve recorded during this experiment is shown in Fig. 11 (a) , a Peak-to-Peak amplitude of 0.1539 mm was obtained using the LDV, whereas in Fig. 10 (a) we presents the one obtained through $ANSYS$ which was equal to 0.16393 mm. we employed a short time interval for a demonstration purpose while the sampling frequency is $2.5KHz$. This sampling rate was shown to be sufficient for sampling up to the 2nd vibration mode. The relative error is 6.4% and it represents the calculated relative error in the amplitudes between the experimental and numerical results while the error in frequency estimation (1st mode of the blade) was less than 0.5% when comparing between $ANSYS$ and the LDV results and about 4% if we compared to the value estimated by the proposed mathematical approach.

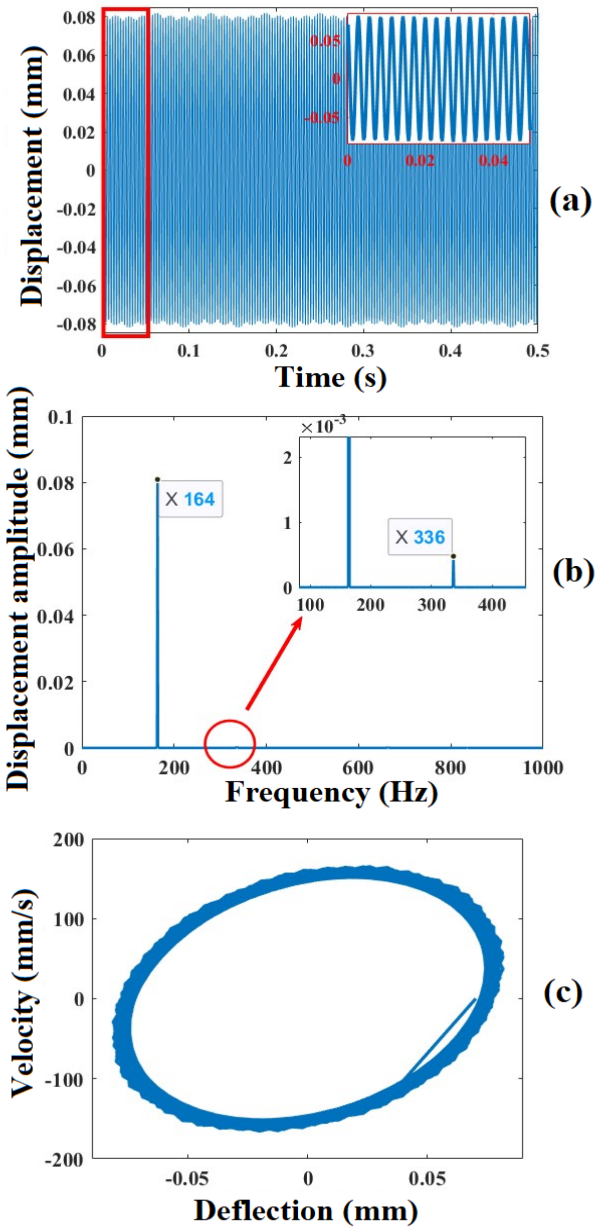

Fig. 10. Simulation results obtained by $ANSYS$ (a): Time evolution of blade's lateral deflection due to the magnetic force generated by the electromagnet supplied by a current with frequency $\omega = 164\ Hz$, (b): Lateral deflection power spectrum and (c): Phase portrait.

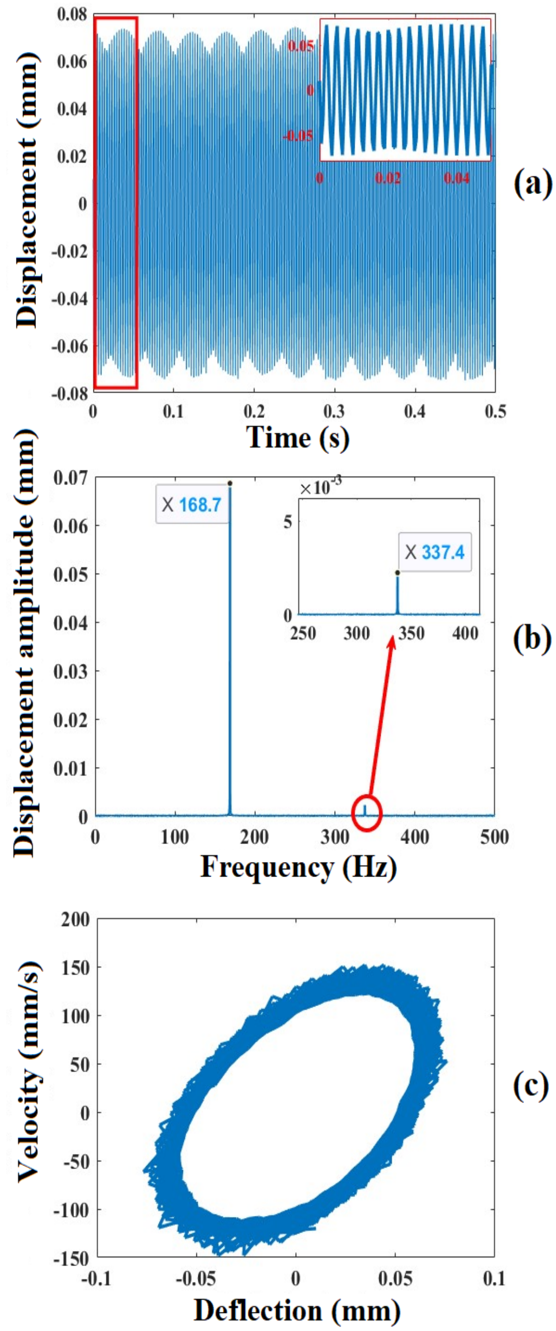

Fig. 11. Experimental results obtained through LDV system (a): Time evolution of blade's lateral deflection due to the magnetic force generated by the electromagnet supplied by a current with frequency $\omega = 164\ Hz$, (b): Lateral deflection power spectrum and (c): Phase portrait.

TABLE I
A COMPARATIVE TABLE FOR THE RESULTS OBTAINED FROM NUMERICAL ANALYSIS, ANSYS AND THE LDV.

	Numerical	ANSYS	Error(%)	LDV	Error(%)
Amplitude (mm)	0.180	0.16393	9.8	0.1539	6.11
Frequency (Hz)	351	336	4.46	337.4	0.416

The Table I shows the results obtained from each model and an overview of the relative error where the simulation results (ANSYS) were taken as a reference. The relative error in amplitudes is justified as per the assumptions mentioned in Section II B. The comparison between the obtained values and the value estimated by the proposed mathematical approach shows a high agreement. The relative error is considered acceptable and neglect the fact that the experimental measurements are affected by an integration error in the LDV signal processing toolbox. The prominence of the spectral component at half the excitation frequency in the power spectrum curves shown in Fig. 11 (b) and Fig. 10 (b) can be attributed to the phenomenon of period-doubling , a nonlinear effect commonly observed in resonant systems. This effect signifies a transition from a stable state to oscillatory behavior, leading to the appearance of spectral components at integer fractions of the excitation frequency. In the context of our experiment with the cantilevered structure excited at its first mode, the observed prominence of the spectral component at half the excitation frequency indicates the presence of this period-doubling phenomenon, emphasizing the significance of nonlinear dynamics in the system's response. The torus-shaped phase portrait resulting from our experimental and simulation studies in Fig. 11 (c) and Fig. 10 (c), with the point of measurement at the blade tip and excitation force close to the resonance, highlights the intricate interplay between the resonance-induced excitation and the system's dynamics. This complex cyclic behavior underscores the involvement of multiple vibrational modes and emphasizes the significance of nonlinear energy exchanges within the system. The agreement between the experimental and simulated results validates the accuracy of our simulations and highlights the robustness of our findings. For the experimental procedure, the potential loading effect from electromagnetic excitation was assessed and considered negligible. We used electromagnetic excitation to generate blade vibrations, measured by a Laser Doppler Vibrometer (LDV) based on the Doppler effect. This non-contact method avoids introducing additional mass or stiffness, eliminating any mechanical loading effect that could alter the blade's dynamic response. The electromagnetic system was precisely controlled to induce the required vibrations without significantly changing the blade's properties. Careful calibration ensured minimal alteration of the blade's characteristics. The control system of the electromagnet, along with real-time monitoring of the blade's vibrations, allowed for consistent and repeatable testing conditions. Please note that the integration error can be easily minimized. However, since we did not study the nonlinearity of the dynamic behavior of the blade, we avoided processing this error in this work.The reason for the error is that the LDV system measures in principle the velocity at any arbitrary target point of the body under study, and the automatic integration producing the blade displacement is biased, which contributes to the discrepancy observed when comparing the methods. In this study, the effect of damping was not considered, since the comparison was made on the same model with different approaches, in order to have an overview of the blade dynamics and to have a reference for the uncertainty evaluation.

IV. Conclusion

In this article, we performed a theoretical and experimental analysis of a blade with an airfoil cross-section subjected to a periodic magnetic force generated by an electromagnet. In the theoretical analysis, we derived the equation describing the motion of the excited blade while considering it as a Timoshenko cantilever beam. The numerical analysis obtained by resolving the blade motion equation for both cases revealed that the blade dynamics exhibit quasi-periodic behavior, with the first mode of vibration and the excitation frequency being the most dominant frequencies. On the other hand, the numerical analysis via ANSYS and the experimental results showed good qualitative agreement in the case of an excitation frequency of 328 Hz. Numerical analysis by directly solving the mathematical equation of the Timoshenko blade showed that it could vibrate with two frequencies.This work forms the foundation for future research related to the utilization of blade tip timing for measuring blade vibration. Thus, by primarily analyzing the system as described, we could estimate the potential frequencies of the blade vibration. The prior knowledge about the vibration signal provided by this paper could assist in optimizing and calibrating the mathematical model for determining the positions of the probes.

V. Acknowledgment

Project No.903141 "Experimental and theoretical research of uncertainties of the Blade Tip Timing Method", Institute of Thermomechanics Academy of Sciences of the Czech Republic; Research program Strategy AV21/27 "Sustainable energetics", Academy of Sciences of the Czech Republic; Academy of Sciences of the Czech Republic; Batista (Blade Tip Timing System Validator) - Clean Sky 2 - 862034, funded by the EU Commission (H2020 CS2).

References

[1] Bérenger Berthoul, Alain Batailly, Laurent Stainier, Mathias Legrand, Patrice Cartraud, "Phenomenological modeling of abradable wear in turbomachines", *Mechanical Systems and Signal Processing*, Vol 98, 2018, pp. 770–785.

[2] Thibaud Plantegenet, Mihai Arghir, Pascal Jolly, "Experimental analysis of the thermal unbalance effect of a flexible rotor supported by a flexure pivot tilting pad bearing", *Mechanical Systems and Signal Processing*, Vol 145, 2020.

[3] Yue, L and Liu, H and Zang, C and Wang, D and Hu, W and Wang, L, "The Parameter Identification Method of Blade Asynchronous Vibration Under Sweep Speed Excitation," *Journal of Physics: Conference seligries*, vol 744,2016, pp.012051.

[4] Lozynskyy, Andriy and Marushchak, Yaroslav and Lozynskyy, Orest and Kasha, Lidiya, "Synthesis of Combine Feedback Control of Electromechanical System by Feedback Linearization Method," *2020 IEEE Problems of Automated Electrodrive. Theory and Practice (PAEP)*, 2020, pp.1–6.

[5] Tchawou, EB and Woafo, P, "Harvesting energy using a magnetic mass and a sliding behaviour," *Nonlinear Engineering Nonlinear Engineering*, vol 3,2014, pp.89–97.

[6] Tékam, GT Oumbé and Tchuisseu, EB Tchawou and Kwuimy, CA Kitio and Woafo, P ,"Analysis of an electromechanical energy harvester system with geometric and ferroresonant nonlinearities," *Nonlinear Dynamics*, vol 76, 2014, pp.1561–1568.

[7] Mekhalfia, Mohammed Lamine, "Optimization of thermal energy harvesting by PZT using shape memory alloy," *Energy Harvesting and Systems*, vol 7, 2020, pp.1–11.

[8] Xu, Hailong and Chen, Zhongsheng and Xiong, Yeping and Yang, Yongmin and Tao, Limin, "Nonlinear dynamic behaviors of rotated blades with small breathing cracks based on vibration power flow analysis," *Shock and Vibration*, vol 2016,2016.

[9] Beauseroy, Pierre and Lengellé, Régis, "Nonintrusive turbomachine blade vibration measurement system," *Mechanical Systems and Signal Processing*, vol 21,2007, pp.1717–1738.

[10] Diamond, DH and Heyns, PS and Oberholster, AJ, "A comparison between three blade tip timing algorithms for estimating synchronous turbomachine blade vibration," *9th WCEAM Research Papers*,2015 pp.215–225.

[11] Endoh, M and Matsuda, Y and Matsuki, M, "Noncontact Measurement of Rotating Blade Vibrations," *Proceedings of the International Gas Turbine Congress, Tokyo, Japan, 1983*,1983, pp.953–960.

[12] Zielinski, M and Ziller, G, "Noncontact vibration measurements on compressor rotor blades," Measurement Science and Technology, vol 11, 2000, pp.847.

[13] Heath, S and Imregun, M, "A survey of blade tip-timing measurement techniques for turbomachinery vibration", 1998 *ASME. J. Eng. Gas Turbines Power*, vol 120, 1998, pp.784–791.

[14] Janicki Grzegorz, Pezouvanis Antonios, Mason B and Ebrahimi MK, ”Turbine blade vibration measurement methods for turbocharges”. *American Journal of Sensor Technology.*, vol 2, 2014, pp.13–19.

[15] Procházka, Pavel, ”Impulse exciter of rotating blades with an increased excitation force,” *IEEE Transactions on Instrumentation and Measurement*, vol 68, 2018, pp.300–302.

[16] Procházka Pavel, ”Methods and Facilities for Calibration of Noncontact Blade Vibration Diagnostic Systems,” *IEEE Transactions on Instrumentation and Measurement*, vol 67, pp.2345–2352, 2018.

[17] Ktena, Aphrodite, ”Physics and Modeling of Magnetic Non Destructive Testing Techniques”, *Materials and Applications for Sensors and Transducers*, vol 495, pp.265–268, 2012.

[18] Procházka Pavel, ”Electromagnetic Simulator of Rotating Machine Blades for Noncontact Sensor Dynamic Testing,” *IEEE Transactions on Instrumentation and Measurement*, vol 67, pp.1506–1508, 2018.

[19] Procházka Pavel and Vanek F., ”Operational Measurement of Stationary Characteristics and Positions of Shrouded Steam Turbine Blades,” *IEEE Transactions on Instrumentation and Measurement*, vol 65, pp.1079–1086, 2016.

[20] Procházka Pavel and Vanek F., ”New Methods of Noncontact Sensing of Blade Vibrations and Deflections in Turbomachinery,” *IEEE Transactions on Instrumentation and Measurement*, vol 63, pp.1883–1592, 2014.

[21] Abdelrhman AM, Hee LM, Leong MS, Al-Obaidi S. ”Condition Monitoring of Blade in Turbomachinery: A Review.” *Advances in Mechanical Engineering*. Vol 6, 2014.

[22] Zhongsheng Chen, Hao Sheng, Yemei Xia, Weimin Wang, Jing He, ”A comprehensive review on blade tip timing-based health monitoring: status and future,” *Mechanical Systems and Signal Processing*, Vol 149, 107330, 2021.

[23] W. J. Staszewski, C. Boller, G. R. Tomlinson, ”Health Monitoring of Aerospace Structures: Smart Sensor Technologies and Signal Processing,” *John Wiley* & *Sons*, Ltd, 2004.

[24] B. Yardimoglu, T. Yildirim, ”Finite element model for vibration analysis of pre-twisted Timoshenko beam,” *Journal of Sound and Vibration*, Vol 273, pp.741-754, 2004.

[25] Selig Michael S, ”UIUC airfoil data site,” *Department of Aerospace Engineering at the University of Illinois*,1996.

[26] Meral Bayraktar,Ali DEMİRTAŞ, ”Free vibration analysis of an aircraft wing by considering as a cantilever beam,” *Selcuk University Journal of Engineering Science and Technology* , vol 7, pp.12–21, 2019.

[27] MB. J. Halkon and S. J. Rothberg, ”Vibration measurements using continuous scanning laser Doppler vibrometry: theoretical velocity sensitivity analysis with applications,” *Measurement Science and Technology*, vol 14, 2003.

[28] S.J. Rothberg, M.S. Allen, P. Castellini, D. Di Maio, J.J.J. Dirckx, D.J. Ewins, B.J. Halkon, P. Muyshondt, N. Paone, T. Ryan, H. Steger, E.P. Tomasini, S. Vanlanduit, J.F. Vignola, ”An international review of laser Doppler vibrometry: Making light work of vibration measurement, Optics and Lasers in Engineering,” *Optics and Lasers in Engineering*, vol 99,pp.12–22, 2017.

[29] Polytech hardware manual, ”Polytec scanning vibrometer PSV-500”. *www.Polytec.com*.